

Heat transfer in a fluidized bed

Nikhil Chitnavis

Indian Institute of Technology Madras, Chennai, Tamil Nadu, India

Abstract

When fluid passes through the bed of solid particles, depending on the rate with which fluid is passing through it, the bed shows some variation in the position of the particles. Due to this variation, it intensifies the mixing of particles, which consequence in an increase in heat transfer. In the present study, hot air is passed through the cold solid bed particles for two different inlet velocities. Based on the air velocity, the heat transfer through the bed is observed. For lower inlet velocity, the bed particles are not getting affected therefore, the heat transfer through the bed is more like conduction heat transfer through solid bed, However, for high velocity, the bed particles shows bubbling effect which increases the heat transfer in the bed and the temperature vary exponentially with time. In the present study, opensource C++ based platform OpenFOAM is used for running the simulations for which solver used is twoPhaseEulerFOAM.

1 Introduction

Fluidization is a process whereby a bed of solid particles is transformed into something closely resembling a liquid. This is achieved by pumping a fluid (either gas or liquid). The fluid is pumped at a rate that is sufficient to exert a force on the particles that exactly counteracts the weight of the particle; in the way, instead of a rigid structure held in place by means of gravity-derived contact forces, the bed acquires fluid-like properties free to flow and deform. There are different types of fluidisation described as: 1.) homogeneous fluidisation

in which particles are separated from each other uniformly due to fluidisation. 2.) Bubbling fluidisation, when the fluid velocity increases gradually and a point reached which cause considerable mixing of the solid particles and gives the appearance of boiling liquid. The major industrial applications for fluidised bed are in catalytic cracking reactor in petroleum refining process, gas fluidisation in chemical reactors, and liquid fluidisation in water treatment, mineral processing and fermentation technology *etc.*

Due to the fluidised nature of the solid particle, lot of research is carried out in this domain. Liu and Hinrichsen[1] used various discretisation scheme for comparison and validation of bubbling fluidised bed using OpenFOAM [2] against the experimental data for uniform gas inlet and central gas jet. The study concluded that the faceLimited gradient scheme makes the convection term more diffusive. Ye et al. [3] investigated the effect of cohesion and drag model on the bed hydrodynamics of Geldart A particles based on two-fluid model. They concluded that for low gas velocity, the effect of cohesion on the bed expansion is relatively small; however, for the higher gas velocity, the bed shows the transition from homogeneous fluidisation to bubbling fluidisation. Wang et al. [4] coupled the CFD-DEM (Discrete Element Method) for the heating of the fluidised heat for the 3D domain and showed the effect of particle size and gas velocity on the heat transfer.

In the present work, heat transfer in the fluidised bed is studied for heating and cooling of the bed and analysed the rate of heat transfer for both the cases.

2 Methodology and Governing Equation

The numerical study is conducted using the open source C++ base toolkit OpenFOAM, which uses finite volume method to discretize the Navier-Stokes equation. For solving the two-phase system, the Eulerian-Eulerian-based mixture model and twoPhaseEulerFoam solver are used for the numerical simulation. The governing equation for the fluid is given below:

Conservation of mass for both phases is given by:

$$\frac{d(\rho_s \alpha_s)}{dt} + \nabla \cdot (\rho_s \alpha_s u_s) = 0 \quad (1)$$

$$\frac{d(\rho_g \alpha_g)}{dt} + \nabla \cdot (\rho_g \alpha_g u_g) = 0 \quad (2)$$

where, s is solid phase and g is fluid phase (either gas or liquid)

Conservation of momentum:

$$\frac{d(\rho_s \alpha_s u_s)}{dt} + \nabla \cdot (\rho_s \alpha_s u_s u_s) = -\alpha_s \nabla p - \nabla p_s + \nabla \cdot (\alpha_s \tau_s) + \rho_s \alpha_s g + F_d \quad (3)$$

$$\frac{d(\rho_g \alpha_g u_g)}{dt} + \nabla \cdot (\rho_g \alpha_g u_g u_g) = -\alpha_g \nabla p + \nabla \cdot (\alpha_g \tau_g) + \rho_g \alpha_g g + F_d \quad (4)$$

Conservation of Energy: (fluid)

$$\frac{d(\rho_g \alpha_g C_{pg} T_g)}{dt} + \nabla \cdot (\rho_g \alpha_g C_{pg} u_g T_g) = \nabla \cdot (\alpha_g \kappa_g \nabla T_g) \quad (5)$$

where C_{pg} and κ_g are the specific heat and the thermal conductivity for the fluid phase.

The solid shear stress (τ_s) and solid pressure (p_s) in Eq. 3 are modelled by the kinetic theory of granular flow (Gidaspow [5]). The fluctuation energy of solid phase, also known as granular temperature is obtained by solving the transport equation

$$\frac{3}{2} \left[\frac{\partial}{\partial t} (\alpha_s \rho_s \Theta) + \nabla \cdot (\alpha_s \rho_s U_s \Theta) \right] = (-p_s I + \tau_s) : \nabla U_s + \nabla \cdot (\kappa_s \nabla \Theta) - \gamma_s + J_{vis} + J_{slip} \quad (6)$$

Where Θ is granular temperature, κ_s is the conductivity of the granular temperature, γ_s is the dissipation rate due to particle collisions, J_{vis} is the dissipation rate resulting from viscous damping, and J_{slip} is the production rate due to slip between gas and particle.

The gas phase is assumed as a Newtonian fluid, and its stress tensor is defined using Newtonian stress-strain relation:

$$\tau_g = \mu_g [\nabla U_g + (\nabla U_g)^T] - \frac{2}{3} \mu_g (\nabla \cdot U_g) I \quad (7)$$

Similarly, the shear stress tensor of solid phase is expressed as

$$\tau_s = \mu_s[\nabla U_s + (\nabla U_s)^T] + (\lambda_s - \frac{2}{3}\mu_s)(\nabla \cdot U_s)I \quad (8)$$

where, μ_s is the solid shear viscosity (viscosity of the solid granules) and λ_s is the solid bulk viscosity (also known as conductivity of the solid granules- which allows the fluid to flow through bulk solid)

Solid shear viscosity is modelled using Gidaspow [5] model:

$$\mu_s = \frac{4}{5}\alpha_s^2\rho_s d_p g_o(1+e) \left(\frac{\Theta}{\pi}\right)^{1/2} + \frac{10\rho_s d_p \sqrt{\Theta\pi}}{96g_o(1+e)} \left[1 + \frac{4}{5}\alpha_s g_o(1+e)\right]^2 \quad (9)$$

Similarly, the solid bulk viscosity is modelled using conductivity model proposed by Gidaspow [5]

$$\lambda_s = \frac{4}{3}\alpha_s\rho_s d_p g_o(1+e) \left(\frac{\Theta}{\pi}\right)^{1/2} \quad (10)$$

Where, d_p is the particle diameter, e is the particle-particle restitution coefficient and g_o is the radial distribution function.

p_s is solid phase pressure is modelled proposed by Lun et al. [6]

$$p_s = \alpha_s\rho_s\Theta[1 + 2(1+e)g_o\alpha_s] \quad (11)$$

Radial distribution function is modelled proposed by Sinclair and Jackson [7]

$$g_o = \left[1 - \left(\frac{\alpha_s}{\alpha_{s,max}}\right)^{1/3}\right]^{-1} \quad (12)$$

Default values: $e = 0.8$, $\alpha_{max} = 0.62$, $\alpha_{min} = 0.5$

Solid frictional pressure model: In the regions where the particles are closely packed, the behavior of the granular flow is dominated by the frictional stresses.

This friction pressure is modelled using Johnson, Nott, and Jackson [8] model:

$$p_{s,f} = Fr \frac{(\alpha_s - \alpha_{s,min})^n}{(\alpha_{s,max} - \alpha_s)^p} \quad (13)$$

$$\mu_{s,f} = \frac{p_{s,f} \sin \phi_{fr}}{2\sqrt{I_{2D}}} \quad (14)$$

Where, $Fr = 0.05N/m^2$, $n = 2$, $p = 5$, ϕ_{fr} is the internal frictional angle ($\phi_{fr} = 28.5^\circ$).

The interphase momentum transfer (F_d) is calculated with drag force. The drag model is proposed by Gidaspow [5].

$$F_d = \begin{cases} 150 \frac{\mu_g \alpha_s^2}{(d_p)^2 \alpha_g} + 1.75 \frac{\rho_g \alpha_s}{d_p} |u_g - u_s|, & \alpha_s \geq 0.2 \\ \frac{3}{4} \frac{C_d \alpha_s \alpha_g \rho_g |u_g - u_s|}{d_p} \alpha_g^{-2.65}, & \alpha_s < 0.2 \end{cases} \quad (15)$$

Drag force Coefficient:

$$C_d = \begin{cases} \frac{24}{Re_p} (1 + 0.15(\alpha_g Re_p)^{0.687}), & \alpha_g Re_p < 1000 \\ 0.44, & \alpha_g Re_p \geq 1000 \end{cases} \quad (16)$$

3 Results and Discussion

3.1 Validation studies

For the present study, the unsteady is discretized using a first-order Euler scheme, and convective and Laplacian terms are discretized using a second-order central difference scheme. An unsteady solver *twoPhaseEulerFoam* is used for the CFD simulations which is *PIMPLE* based solver for all the cases with the time step of $0.0001s$. *PIMPLE* solver is a combination of *SIMPLE* (Semi Implicit Method for Pressure Linked Equation) and *PISO* (Pressure-Implicit with Splitting of Operators), where the advantages of both the solvers is utilized. Further, the pressure matrices is solved using pre-conditioner conjugate gradient solver and the velocity is solved using gauss-seidel method. The convergence criteria for both velocity and pressure is kept at 1×10^{-6} . The present study is solved using a two-phase based Eulerian-Eulerian model therefore, alpha (void fraction, α) is also considered and discretized using vanleer second order scheme, and is solved using Gauss seidel method.

For the validation study, the solver is compared against the numerical results of Ye et al. [3] for a 2D case with a uniform gas velocity at the inlet by considering the particle size of

$65\mu m$. The details of the validation test is given in Table 1 and the boundary condition is showed in Figure 1.

Table 1: Details for the validation test case.

S.No.	Parameters	Value
1.	Superficial air inlet velocity (U_{air})	$0.06m/s$
2.	Intial bed height (H_o)	$1.2m$
3.	Initial void fraction ($\alpha_{particles}$)	0.56
4.	Initial void fraction (α_{air})	0.44
5.	particle diameter (d_p)	$65\mu m$
6.	Particle density	$1780kgm^{-3}$

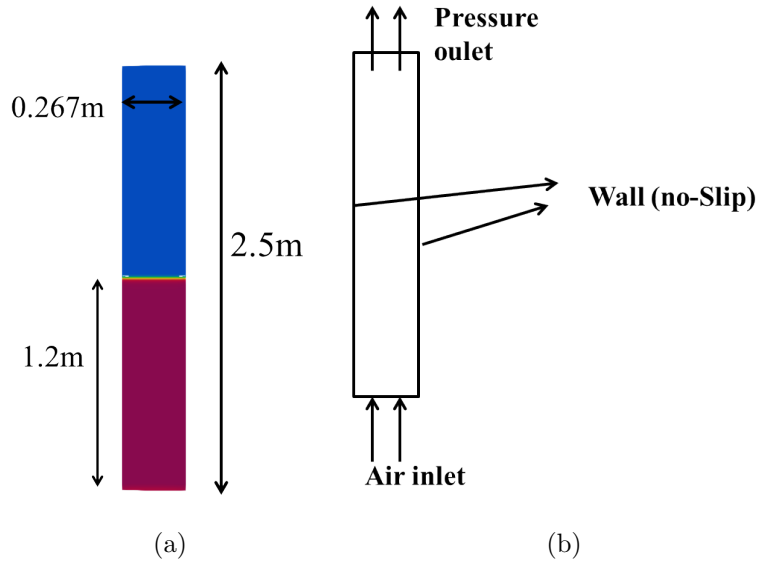


Figure 1: a.) Geometric detail b.) Boundary condition

The axial variation (along the height) of the void fraction is compared against the data of Ye et al. [3]. The present study showed the comparison of solid void fraction variation for three different drag model as shown in Figure 2. In comparison, the drag model of Gidaspow [5] shows a considerable match against the data.

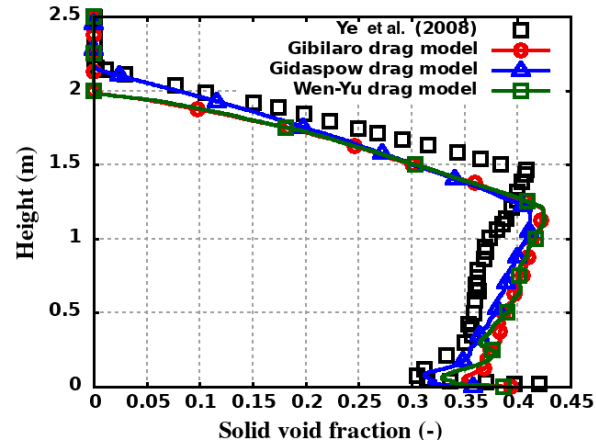


Figure 2: Comparison of the solid void fraction along the height of the domain against the data of Ye et al. [3].

3.2 Geometric detail and boundary condition for the test case

The 2D simulation is performed for the fluidised bed for the present study, using cooling and heating of the fluidised bed. The temperature variation of the bed and heat transfer coefficient is compared with respect to time. The geometric details and boundary conditions is given below in figure 3. The initial height of the bed is $0.4m$ and the simulation is performed for two different velocities to analyse the effect of inlet air velocity on the heat transfer rate.

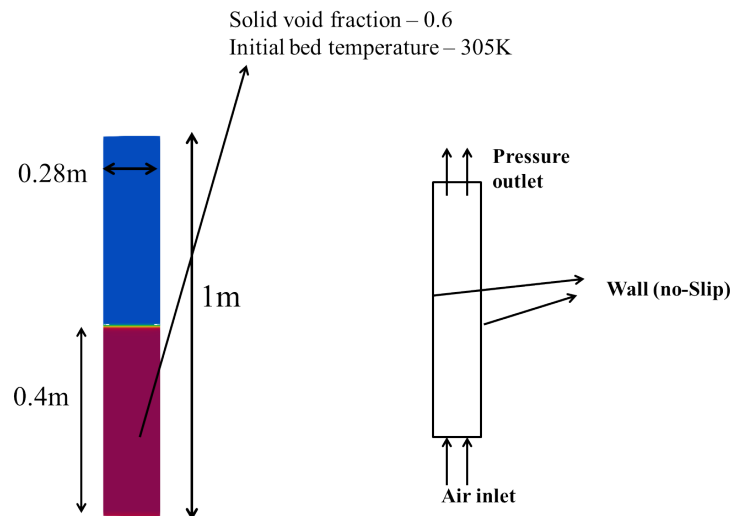


Figure 3: Geometric detail and boundary condition for the test cases (condition is shown for cooling of fluidized bed)

For the case of cooling of fluidized bed the difference in temperature inlet air and the bed is $5K$, however for the heating of fluidized bed case the difference in temperature in $10K$. Further, the simulation is performed for two set of inlet air velocity *i.e.*, $0.46m/s$ and $0.1m/s$. The grid independency is performed to get the optimum mesh for the present study.

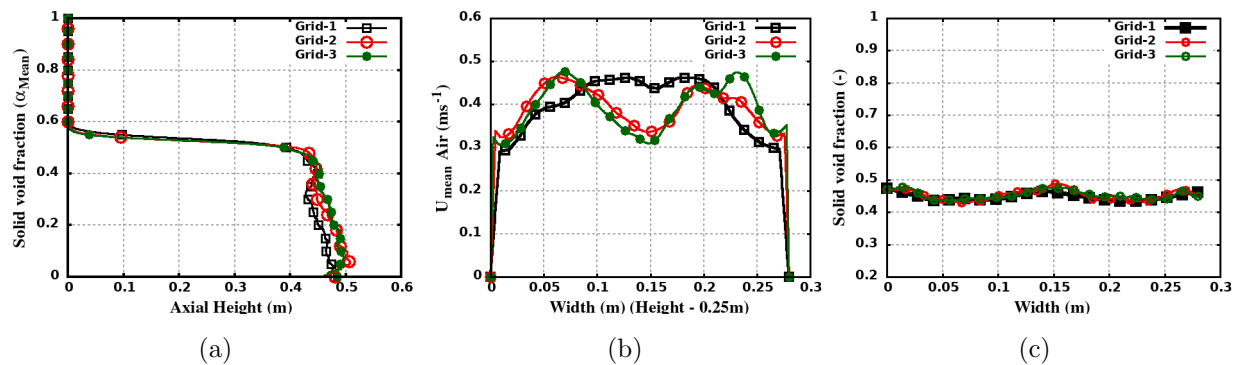


Figure 4: Grid independency for the present study.(a) axial variation of solid void fraction (b) mean air velocity and (c) solid void fraction along the width of channel.

The simulation is performed for three different grid *i.e.*, Grid 1 is $11k$ mesh element, Grid 2 has $22k$ mesh element and Grid 3 has $44k$ mesh elements. The grid-independent study is shown in Figure 4 where the solid void fraction along and across the channel and mean air velocity along the width is compared for three different grids. From the comparison, the results of Grid-2 and Grid-3 are comparable to each other. Therefore for the present study Grid-2 will be considered.

3.3 Heating of the fluidised bed.

For the heating of the fluidised bed, the hot air is passed from the inlet, keeping the bed temperature less than the air temperature. The geometric details and the boundary conditions are shown in Figure 3. The simulation is performed for the two different air velocity, case1 having a inlet air velocity of $0.46m/s$ and case2 with velocity of $0.1m/s$. The initial bed temperature is at $300K$ and the inlet air temperature is maintained at $310K$, keeping the difference in inlet air temperature and bed temperature constant *i.e.*, $10K$.

The details of the solid bed and initial condition is given in Table 2

Table 2: Details for the validation test case.

S.No.	Parameters	Value
1.	Superficial air inlet velocity (U_{air})	0.10 , 0.46m/s
2.	Initial bed height (H_o)	0.4m
3.	Initial void fraction ($\alpha_{particles}$)	0.60
4.	Initial void fraction (α_{air})	0.40
5.	particle diameter (d_p)	280 μ m
6.	Particle density	2500kgm ⁻³
7.	Probe locations	0.2, 0.3, 0.4, 0.5m

In the present study, the variation in bed temperature is compared at different probe locations over a period of time. The locations for the probe are shown in Table 2. As the hot air enters the bed, the bed temperature gradually increases. Depending on the inlet velocity of the air, bed behaviour can change. For low velocity, the bed will not show any fluidisation; only the temperature of the bed will change. Once the inlet air velocity is equal to or greater than the minimum fluidisation condition, the bed will come in a fluidised state. The fluidisation of the bed ensures the faster mixing of bed particles, resulting in faster heat transfer. The effect of air velocity discussed above is shown in Figure 5. The simulations are performed for the time period of 200seconds for both cases. In Case-(a) (Figure 5a), the temperature of the bed gradually increases without any fluctuation, however in Case-(b) (Figure 5b), the bed temperature shows fluctuations and the rate of rise in bed temperature for Case-(b) (Figure 5b) is also higher compared case-(a). For the same time periods the bed temperature of Figure 5b has reached 301.5K, however for Figure 5a it has reached 301.2K.

The same heat transfer behaviour of the bed can be explained from Figure 6, where Figure 6a shows the constant value of non-dimensional heat transfer coefficient (*i.e.* bed has not reached the state of fluidisation), however, Figure 6b shows the significant fluctuations in the non-dimensional heat transfer coefficient which signifies the bed has reached the state of fluidisation which result in higher mixing of bed particles hence increases heat transfer in Case-(b) (*i.e.* inlet air velocity of 0.46m/s).

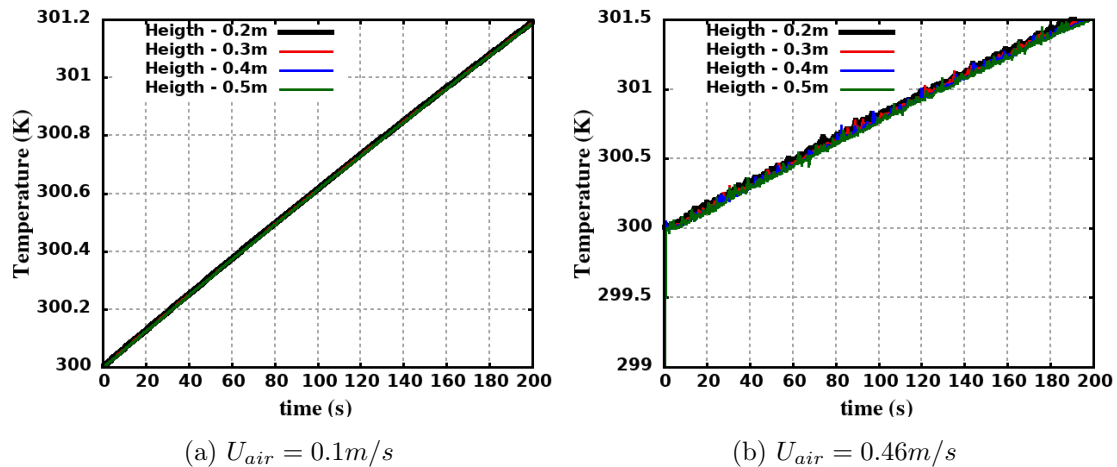


Figure 5: Comparison of bed temperature at various probe locations by varying the inlet air velocity.

Figure 7 shows the variation of the solid void fraction of the bed at different time periods for the uniform air inlet of $0.46m/s$. At higher air inlet velocity, the bed particle got lifted up by the air, giving the appearance of a fluid boiling process. This bubbling effect in the bed increases the rate of heat transfer.

3.4 Cooling of the fluidised bed.

Similar to the heating of the fluidized bed, here, in the case of cooling of the bed, is at a higher temperature, and the inlet air is at a low temperature. The geometric details and the boundary conditions are shown in Figure 3 with the initial bed temperature of $305K$, and the inlet air temperature is maintained at $300K$. Further, the simulation for cooling of the bed is only performed for the higher air inlet velocity of $0.46m/s$.

Figure 8 shows the variation of bed temperature of the period of 50s for which the drop in temperature is $0.2K$. Figure 8 shows the temperature variation at various probe locations (the location of the probes is given in Table 2), for the probe location of $0.2m$ (measured from the inlet), the fluctuation in temperature is least compared to the temperature variation at other probe locations.

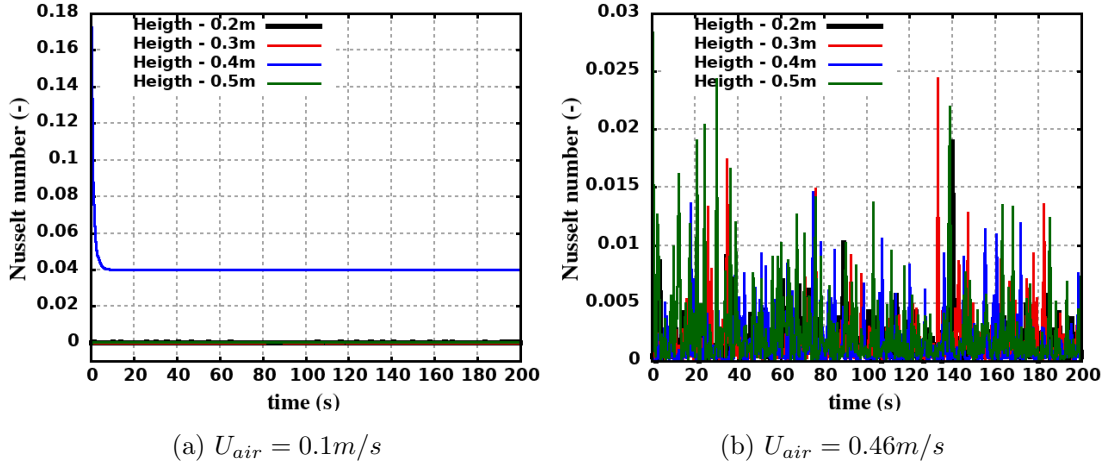


Figure 6: Comparison of bed heat transfer coefficient at various probe locations by varying the inlet air velocity.

3.5 Calculation of time constant

In the present study of heat and cooling of the fluidized bed, the bed temperature will gradually reach the inlet air temperature. However, this change in the bed temperature is not linear with respect to time. To show the variation of temperature change of the bed with respect to time, the time constant equation is calculated for a single particle. Using the conservation of energy, the change in temperature of a single particle is equal to the heat transfer using convection, as shown in equation 17

$$mC_p \frac{dT}{dt} = hA(\Delta T) \quad (17)$$

where m is the mass of the bed particle, C_p is the specific heat of the particle, T is the particle temperature, h is the convective heat transfer coefficient, A is the surface area of the particle, and ΔT is the difference in temperature of bed and the inlet fluid.

Rewriting the equation 17 in non-dimensional form:

$$mC_p \frac{d\theta}{dt} = hA(\theta) \quad (18)$$

where, $\theta = \frac{T - T_{air}}{\Delta T_{max}}$

further rearranging the equation 18,

$$\frac{d\theta}{\theta} = \frac{hA}{mC_p} dt \quad (19)$$

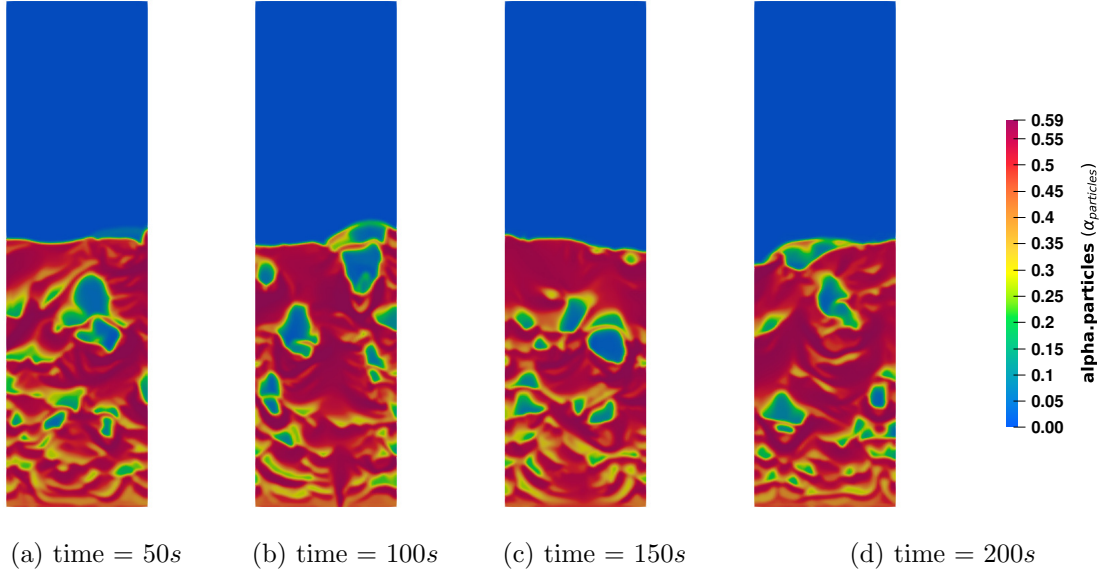


Figure 7: Shows the variation of bed void fraction at different time steps for the uniform air inlet velocity of $0.46m/s$.

However, $\frac{hA}{mC_p}$ is time constant and can be represented using $\tau(s^{-1})$.

$$\therefore \frac{d\theta}{\theta} = \tau dt \quad (20)$$

After solving equation 20 (ODE)

$$\theta = \exp(\tau t + C) \quad (21)$$

On applying the boundary condition for getting the value for constant C in equation 21 is: for t (time) = 0, $\theta = 1$ (non-dimensional temperature), therefore from equation 21, $C = 0$.

$$\theta = \exp(\tau t) \quad (22)$$

Equation 22 shows that for a single particle, the temperature varies exponentially with respect to time. Further, to calculate the time constant value, particle size (diameter), density of the particle and thermophysical properties of air and particle are given in table2. Also, to calculate the heat transfer coefficient (heat transfer from the particle to the surrounding fluid), Ranz and Marshal [9] correlation (Equation 23).

$$h_{cond} = \frac{k_l}{d_p} (2 + 0.6Re^{0.5} Pr^{0.3}) \quad (23)$$

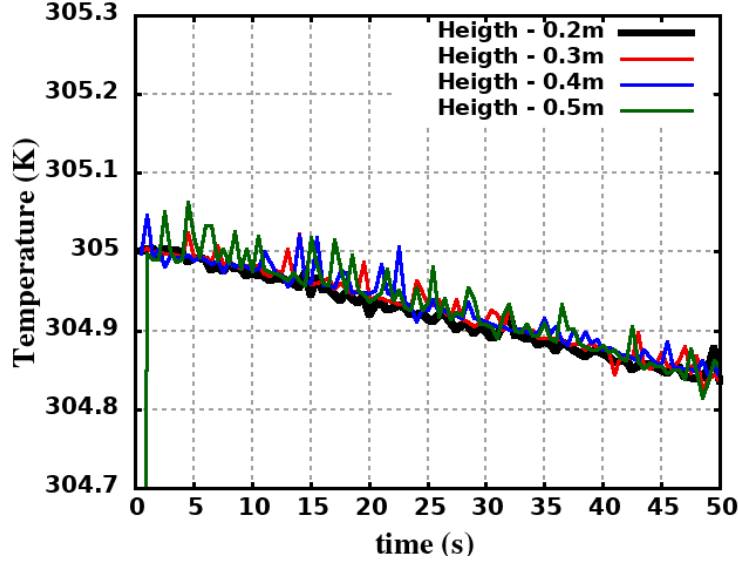


Figure 8: Comparison of bed temperature at various probe locations for the inlet air velocity of 0.46m/s .

where d_p is the particle diameter. Using Equation 23, surface area and specific heat of the particle, the time constant is calculated as:

$$\tau = \frac{h_{cond}A}{mC_p} = \frac{6h_{cond}}{\rho_{particle}d_pC_p} = 0.44697\text{s}^{-1} \quad (24)$$

Using equation 24, equation 21 is re-written as:

$$\theta = \exp(0.44697t) \quad (25)$$

The calculation shown for the temperature variation with respect to time is for a single particle; however, for the bed of particles, the bed temperature variation will be almost the same. Figure 9 shows the trend of temperature variation. The simulation is done for the 1600s with 8 processors, and it took more than 7 days to run this study. Running the simulation for more time steps can clearly show the plateau, *i.e.*, the bed temperature asymptotically reaching the air temperature. Figure 5 shows the temperature variation for the simulation time of 200s, which shows the linear change in the temperature of the bed. however, after running it for more time steps, it shows the variation of bed temperature with respect to equation 25.

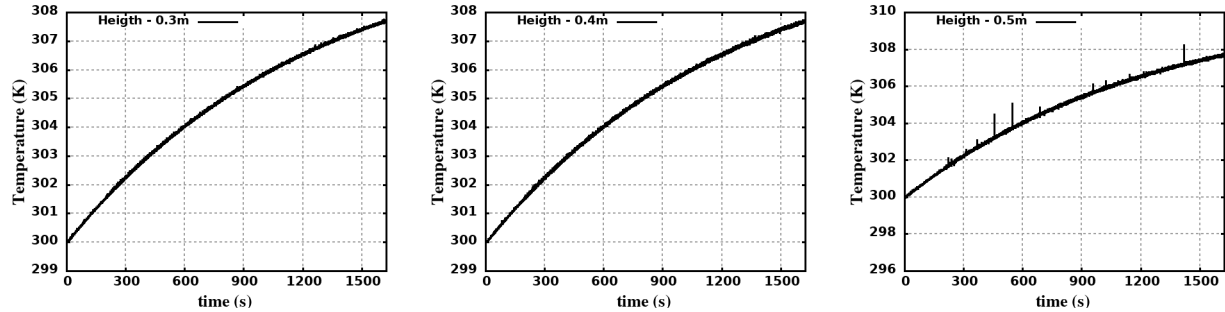


Figure 9: Temperature variation with respect to time at three different probe locations.

4 Conclusions

In the present study, the simulation of the heating and cooling of a fluidized bed is performed and tried to analyse the effect of inlet air velocity on the rate of heat transfer of the bed. With the increase in the inlet air velocity, there is an increase in fluidisation of the solid, which in turn increases the heat transfer of the bed. When the inlet velocity is less than the velocity required for fluidisation, the bed acts as a single solid bed and the heat transfer from the bed is in the form of conduction. However, when the velocity is higher than the minimum fluidisation velocity, the air lifts the solid particle and separates them and gives the appearance of boiling of fluid. This will increase the mixing of solid particles and in turn increases the heat transfer. Further, the variation of bed temperature with respect to time can be misunderstood as a linear variation for a small step. However, after running for 2000s, variation shows an exponential trend.

References

- [1] Yefei Liu and Olaf Hinrichsen. “CFD modeling of bubbling fluidized beds using OpenFOAM®: Model validation and comparison of TVD differencing schemes”. In: *Computers & chemical engineering* 69 (2014), pp. 75–88.
- [2] Hrvoje Jasak, Aleksandar Jemcov, Zeljko Tukovic, et al. “OpenFOAM: A C++ library for complex physics simulations”. In: *International workshop on coupled methods in numerical dynamics*. Vol. 1000. Dubrovnik, Croatia). 2007, pp. 1–20.
- [3] Mao Ye et al. “Two-fluid modeling of Geldart A particles in gas-fluidized beds”. In: *Particuology* 6.6 (2008), pp. 540–548.
- [4] Shuai Wang et al. “CFD-DEM simulation of heat transfer in fluidized beds: Model verification, validation, and application”. In: *Chemical Engineering Science* 197 (2019), pp. 280–295.
- [5] Dimitri Gidaspow. *Multiphase flow and fluidization: continuum and kinetic theory descriptions*. Academic press, 1994.
- [6] Cli KK Lun et al. “Kinetic theories for granular flow: inelastic particles in Couette flow and slightly inelastic particles in a general flowfield”. In: *Journal of fluid mechanics* 140 (1984), pp. 223–256.
- [7] JL Sinclair and R Jackson. “Gas-particle flow in a vertical pipe with particle-particle interactions”. In: *AIChE journal* 35.9 (1989), pp. 1473–1486.
- [8] Paul Carr Johnson, P Nott, and R Jackson. “Frictional–collisional equations of motion for particulate flows and their application to chutes”. In: *Journal of fluid mechanics* 210 (1990), pp. 501–535.
- [9] WE Ranz and Marshal. “Evaporation from drops, Parts I & II”. In: *Chem Eng Prog.* 48 (1952), pp. 141–146.